

Advanced Physics Lab for Physicists

F98: SQUIDs and Noise Thermometers

July, 2024
Kirchhoff Institute for Physics, Heidelberg University

Contents

1	Introduction	3
2	Theory	4
2.1	Superconducting Quantum Interference Devices	4
2.1.1	Superconductivity	4
2.1.2	Flux Quantization	7
2.1.3	Josephson effect and Josephson Junction	9
2.1.4	Voltage State of a Josephson junction	11
2.1.5	Josephson junction in magnetic fields	14
2.1.6	dc-SQUIDs	16
2.2	Noise Thermometers	18
2.2.1	Thermal Noise	19
2.2.2	Principle of noise thermometry	21
3	Methods	25
3.1	dc-SQUID Characteristics	25
3.2	Flux-Locked-Loop	27
3.3	Two-Stage SQUID-Readout	27
3.4	Temperature measurement using a noise thermometer	28
3.4.1	Uncertainty of the calculated temperatures	30
4	Setup	31
4.1	Experimental Setup	31
4.2	SQUID Viewer	32
4.3	PicoScope	34

5 Experiments	37
5.1 Preparations	37
5.2 Single Stage SQUID	37
5.2.1 Open Loop	37
5.2.2 Flux Locked Loop	38
5.2.3 SQUID Noise	39
5.3 Two-stage SQUID Readout	40
6 Outlook	41
6.1 State of the art noise thermometers	41
6.1.1 Signal processing of the C3NT	42

1 Introduction

During this advanced physics lab course, you will read out a noise thermometer with a two-stage SQUID amplifier circuit, both cooled in a liquid helium can at roughly 4K. You will learn a few basics about low-temperature physics and cryogenic liquids, as well as macroscopic quantum effects like superconductivity and superfluidity, while discussing and preparing the experiments with your tutor. Besides an introduction to SQUIDs and noise thermometers, this manual provides several experiments that will teach you how to operate dc SQUIDs as amplifiers in flux-locked-loop mode and obtain the temperature of a resistance from its noise.

SQUIDs (superconducting quantum interference devices) are very sensitive magnetometers that can detect tiny variations in the magnetic field. These SQUIDs are built upon a superconducting loop which is either interrupted by one Josephson junction, the rf-SQUID, or interrupted by two Josephson junctions, the dc-SQUID. The working principle of SQUIDs are based on the Josephson effect as well as the flux quantization of superconducting loops. A Josephson junction can be realised by a superconductor-isolator-superconductor contact, as it is the case for the SQUID of this lab course. A dc SQUID can be used to amplify a small current change into a voltage change. Thus, you will use SQUIDs to read out a noise thermometer. The niobium SQUIDs used during this lab course were fabricated in our cleanroom and are optimized to read out our low-temperature X-ray detector arrays based on MMCs (metallic magnetic calorimeters) in a two-stage flux-locked-loop circuit.

Noise thermometers can determine the temperature from the current noise density of a resistance, which is a result of the Brownian motions of the electrons. They do not need calibration due to their fundamental dependency on physical properties. More importantly, they can be used to measure the temperature over a very large range across multiple orders of magnitude at very low temperatures. During this lab course, you will measure the noise of an aluminum wire and fit the expected current noise density to the measured noise spectrum to determine the temperature.

2 Theory

To be able to understand the later described devices used during this lab course, it is necessary to have some basic knowledge of superconducting quantum interference devices and noise thermometers. This section will start with an introduction to the physical theories necessary to understand the working principle of superconducting quantum interference devices. Afterwards the fundamental physics behind noise thermometers is explained.

2.1 Superconducting Quantum Interference Devices

2.1.1 Superconductivity

The investigation of resistances at very low temperatures and thus the discovery of superconductivity was possible by the achievements of Heike Kamerlingh Onnes to liquefy helium. This achievement allowed for measurements down to near absolute zero temperature by evaporation cooling of liquid helium. Onnes studied samples made out of gold and platinum. He found that the resistance of both metals is approaching a finite value. This finite value depends on the purity and quality of the sample. From this observations he concluded that, ideally, samples should have a vanishing small resistance at lowest temperatures. During the time of H.K. Onnes the only metal that was available in very high purity was mercury, therefore he continued his studies with high purity mercury samples. In 1911 Onnes observed a sudden jump of the resistance for mercury below a certain temperature. The result of this measurement are shown in figure 1.

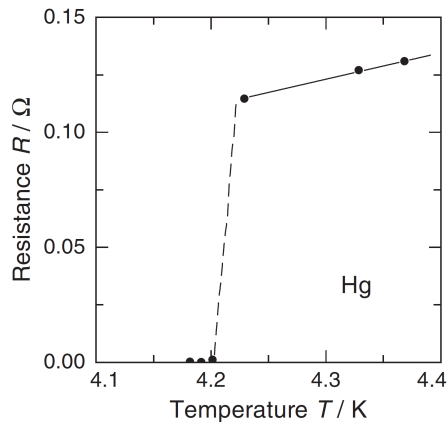


Figure 1: Sudden drop of the resistance of mercury at a critical temperature T_C [5].

From his measurements H.K. Onnes defined a new state of matter, called superconductivity: Superconductivity is the vanishing electrical resistance below a certain transition temperature T_C .

Meißner-Ochsenfeld-Effect From the above definition of superconductivity, a superconductor looks like a perfect conductor. However it turns out that a superconductor is not just a perfect conductor. To have a closer look at this, it is assumed that below a certain temperature T_C the conductor switches to the superconducting or perfect conducting state. Figure 2 shows the two different possibilities of changing the temperature of a perfect and a superconducting sample within a magnetic field.

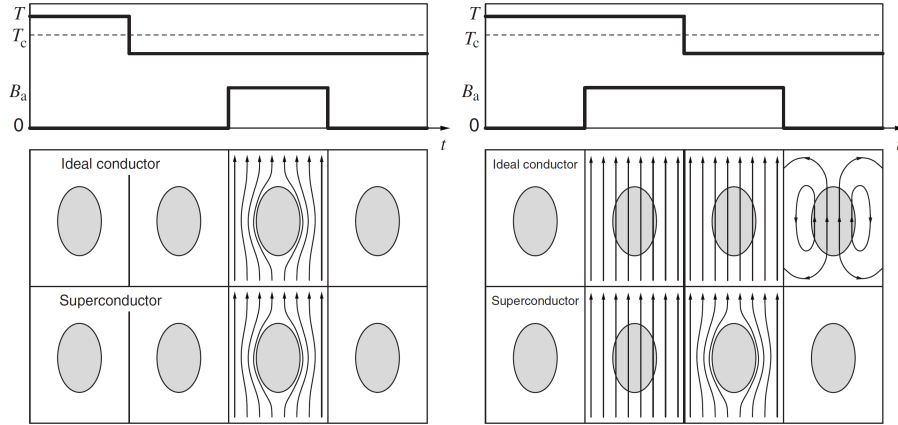


Figure 2: Comparison of the behavior of a perfect conductor and a superconductor in a magnetic field [5]. Left: the magnetic field is switched on after cooling below T_C . Right: samples are cooled below T_C after the magnetic field is switched on.

In both cases displayed above the samples are cooled down below the critical temperature T_C , but in case of the left figure, the magnetic field is switched on after cooling below T_C , whereas in case of the right figure, the field is switched on before the transition to the superconducting state. At the end, the external field is switched off in both cases. For the sequence displayed on the left side of figure 2, switching on the magnetic field induces screening currents at the surface of the samples for both, the superconductor and the perfect conductor. These Lenz screening currents produce a magnetic field (in the Maxwell equations we would treat it as magnetization \mathbf{M}) opposite in direction and equal in size to the internal magnetic field \mathbf{H}_i inside the sample, leading to a vanishing magnetic flux density \mathbf{B}_i inside the sample. After turning off the magnetic field everything returns to the initial state.

Let's now look at the experimental sequence on the right side, where a magnetic field is turned on at a temperature $T > T_C$ at which both samples are still in the normal conducting state. Both samples are then cooled down below T_C , leading to very different magnetic field configurations. For the perfect conductor cooling through T_C doesn't change anything, because only changes of the magnetic flux density, $\frac{\partial \mathbf{B}}{\partial t} \neq 0$, can induce Lenz currents. In contrast, when cooling a real superconducting material exposed to a magnetic field from its normal to its superconducting state, it spontaneously expels magnetic flux density from its volume by starting screening currents beneath its surface, just like the ones that are produced in the sequence on the left side. This spontaneous

expelling of field on cooling through T_C is called Meißner-Ochsenfeld Effect. When turning off the magnetic field, the magnetic flux density inside the superconductor remains zero. In contrast, in the perfect conductor screening currents are now induced according to Lenz's law, which conserve the magnetic flux density.

We summarize: Superconductors (of type-I) are not only perfect conductors, but also perfect diamagnets up to a material-dependent critical field H_C .

BCS-Theory The breakthrough in the theoretical understanding of superconductivity, was achieved in 1957 by the theory of John Bardeen, Leon Cooper, and John Robert Schrieffer, known as the BCS theory. According to this theory, electrons condense pairwise into a new state in which they are described by a well defined common macroscopic wave-function. The theory itself emerged in two steps:

1. Cooper proved that two electrons at the surface of the Fermi sphere can form a so called cooper pair in case that there is an attractive interaction between them. Independent of the strength of the interaction between the two electrons, at low enough temperature those pairs would be stable and have an energy lower than the Fermi Energy leading to the formation of a gap in the energy landscape.
2. Bardeen, Cooper and Schrieffer applied many-body quantum mechanics to show that N electrons forming Cooper pairs condense in a bosonic state described by a single macroscopic wave function.

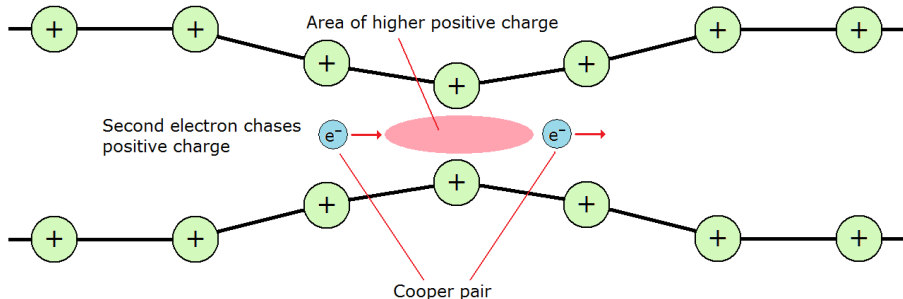


Figure 3: Schematic drawing of the attractive interaction between two electrons. The interaction is mediated by the exchange of a phonon between the two electrons.

Important note: in reality, the electrons of a Cooper pair have opposing k-vectors, in contrast to the electrons depicted here.

Knowing that two electrons, being both negatively charged, repel each other, how can we motivate an attractive force between conduction electrons in a solid? As sketched in figure 3, the negative charge of one electron attracts the positively charged ion-cores within a lattice. This attraction leads to a movement of the ions towards the electron's track. The fact that the speed of the electron is much faster than the movement of the ions the maximum positive charge carrier density is reached when the electron is far

away. The excess of positive charge density then attracts another electron. As the first electron is already far away and as there are many electrons in between, the Coulomb interaction of the two electrons is strongly suppressed, making it possible, that the small attractive force caused by the distortion of the lattice can dominate. Note that this is a very simplified model and does not necessarily describe the real behaviour of the material but is meant to give an intuition of how an attractive interaction could be possible. In the framework of the BCS-theory the attractive interaction is mediated by the exchange of a virtual phonon. This existence of an attractive force between the fermions is the necessary ingredient, which leads to the formation of Cooper pairs, makes the Fermi-gas state become unstable and causes a phase transition into the BCS state.

Properties of Cooper pairs As electrons are fermions, the wave function needs to be antisymmetric on the exchange of two fermions. In simple elemental superconductors the spins of the two electrons couple to the singlett state, $S = 0$, being antisymmetric on the exchange of two electrons. Accordingly the quantum number of the angular momentum needs to be even, and $L = 0$ is energetically preferred in elemental superconductors. In addition we can state that Cooper pairs are composite Bosons with a mass of $M_{\text{CP}} = 2 m_{e^-}$ and a charge of $Q_{\text{CP}} = 2 q_{e^-}$. Below T_c all these bosonic pairs are described by the same macroscopic ground-state wave function:

$$\Psi = \Psi_0 e^{i\phi(\mathbf{r})}. \quad (1)$$

The $\phi(\mathbf{r})$ describes the phase of the wave function. From this common quantum mechanical wave function that describes the Cooper-Pairs within a superconductor two important effects follow: *i*) the flux quantization within a superconducting loop and *ii*) the Josephson-effect. These two effects will be described in the following sections.

2.1.2 Flux Quantization

To explain the flux quantization, one has to look at a closed loop made of a superconducting material. An example for such a loop is shown in figure 4. The loop is cooled below T_C while being exposed to a magnetic flux density B . At the superconducting transition the magnetic field-lines are expelled from the volume of the superconducting ring material, but not from within the loop. This is due to the Meissner effect, in which a surface current is induced to expel the magnetic flux inside of it. At the same time a magnetic field \mathbf{H} penetrates the superconducting material within the London penetration depth of the surface causing a magnetisation. While the surface supercurrents, which do not decay in time, shield the internal part of the superconductor from magnetic flux, there is a finite magnetic field at the surface which is not canceled, leading to an effective finite magnetic field inside the ring. When the external magnetic field is then switched off, the flux through the loop becomes trapped inside the loop, as the magnetic flux density lines are not allowed to penetrate the superconductor when it is in the superconducting state. Screening currents build up beneath the surfaces of the ring in order to conserve the enclosed magnetic flux.

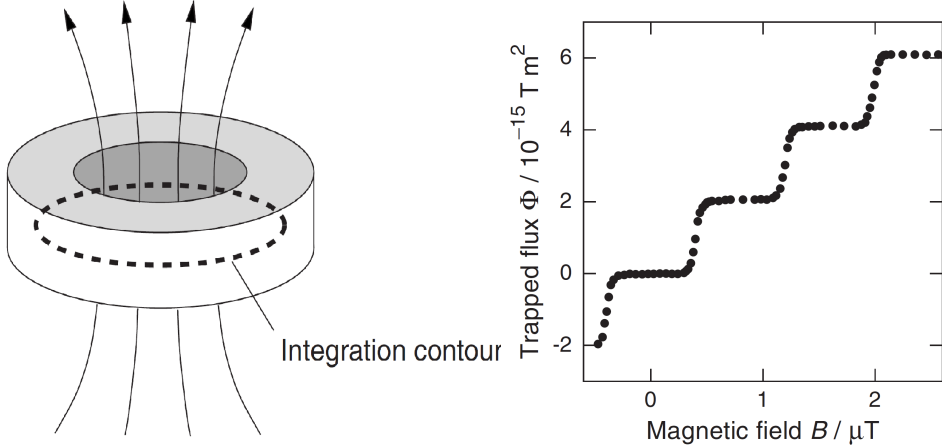


Figure 4: Left: Superconducting loop penetrated by a magnetic flux [5]. Inside the loop the closed integration line is displayed. Right: Magnetic flux trapped within a hollow superconducting cylinder [5]. Depending on the magnetic field, a flux of integer multiple of Φ_0 is trapped.

The phase difference $\Delta\phi$ between two points 1 and 2, along a certain contour is defined by the integral

$$\Delta\phi = \int_1^2 \nabla\phi(\mathbf{r}) \cdot d\mathbf{s}. \quad (2)$$

In case of the superconducting loop shown in figure 4 the integration contour is closed. Using this and the fact that the wave function of a superconductor needs to be well defined, we find that the phase difference needs to be 0 or multiples 2π , $\Delta\phi = 2\pi n$. To calculate the flux trapped within the loop shown in figure 4, the equation

$$\mu_0 \lambda_L^2 \oint_L \mathbf{j} d\mathbf{s} = \frac{\hbar}{e} \oint_L \nabla\phi \cdot d\mathbf{s} - 2 \oint_L \mathbf{A} d\mathbf{s} \quad (3)$$

can be evaluated along a closed contour L deep inside the superconducting ring, where the current density is $\mathbf{j} = 0$, to fulfill $\mathbf{B}_i = 0$. In equation 3, $\lambda_L = \sqrt{\frac{m}{\mu_0 n q^2}}$ stands for the London penetration depth and \mathbf{j} for the current density. Using equation 3 and Stokes theorem, it is possible to solve for the magnetic flux enclosed by the superconducting ring and we find

$$\Phi = n \frac{\hbar}{2e} = n\Phi_0. \quad (4)$$

Here, Φ_0 represents the magnetic flux quantum $\Phi_0 = h/2e = 2,067 \cdot 10^{-15} \text{ Wb}$ [5]. According to equation 4, the magnetic flux within a superconducting loop is an integer

multiple of the magnetic flux quantum Φ_0 . This quantization was experimentally proofed and the result of an experiment with a short piece of superconducting tube is displayed in figure ??:

2.1.3 Josephson effect and Josephson Junction

Another important effect resulting from the fact that the Cooper pairs in a superconductor are described by one unique macroscopic wave function is the so called Josephson-effect. This effect was predicted by Josephson in 1962. To discuss the Josephson effect we want to consider two superconductors separated by a very thin insulating barrier, as sketched in figure 5.

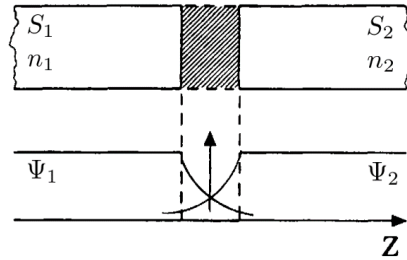


Figure 5: Josephson junction made of two superconductors separated by a very thin insulating barrier. In both superconductors, S_1 and S_2 , the Cooper pairs are described by a unique wave function Ψ_1 and Ψ_2 , respectively. The numbers n_1 and n_2 represent the density of Cooper pairs on the respective side.

For both superconductors, as well as generally for two coupled systems, it is possible to set up a Schrödinger equation:

$$i\hbar\dot{\Psi}_1 = \mu_1\Psi_1 + \kappa\Psi_2 \quad i\hbar\dot{\Psi}_2 = \mu_2\Psi_2 + \kappa\Psi_1. \quad (5)$$

In both equations the Ψ_1 and Ψ_2 represent the wave function of the respective superconductor, whereby their chemical potential is described by μ_1 and μ_2 . The κ in both equations corresponds to the coupling between both superconductors and is determined by the width of the barrier between them.

To solve these two equations, the following assumptions have to be made: The chemical potentials μ_1 and μ_2 of both superconducting electrodes are equal in case of no voltage V applied across the contact. In case of a non zero voltage $V \neq 0$ the relation between the chemical potentials is given by $\mu_2 - \mu_1 = -2eV$. Regarding the density of Cooper-Pairs in both superconductors one can assume n_1 and n_2 to be equal and given by n_s , if both superconducting electrodes are made of the same material.

Inserting the unique wave function given in equation 1, results in two equations:

$$\dot{n}_{s_1} = \frac{2\kappa}{\hbar}n_s \sin(\phi_2 - \phi_1) = -\dot{n}_{s_2} \quad (6)$$

$$\hbar (\dot{\phi}_2 - \dot{\phi}_1) = -(\mu_2 - \mu_1) = 2eV. \quad (7)$$

Here, the difference between the phases of both superconductors could be identified as the phase difference $\Theta = \Phi_1 - \Phi_2$.

Equation 6 is describing a time dependent change of the density of Cooper pairs and therefore of charge carriers. Such a change of charge carriers can be associated with a current I_S . By introducing the critical current $I_0 = n_s 2\kappa / \hbar$ of a Josephson contact, equation 6 can be rewritten:

$$I_S = I_0 \sin(\Theta). \quad (8)$$

This equation is called *first Josephson equation* and describes the phase dependency of the electrical dc current through a Josephson contact. Therefore, the behavior is called *dc Josephson effect*.

In the case that the voltage drop across the barrier is non zero, the behavior of the contact changes according to equation 7. This leads to time-dependent evolution of the phase difference between both superconducting electrodes. The evolution is described by the *second Josephson equation*:

$$\dot{\Theta} = \frac{2eV}{\hbar} = \omega_j. \quad (9)$$

According to the equation, the phase change is given by a frequency ω_j , the Josephson frequency. Due to this and according to equation 8 the current flowing through the contact is also changing with the Josephson frequency. Therefore this behavior is called *ac Josephson effect* [8].

Non Linear Behaviour of a Josephson Junction As discussed above the two wave functions of both superconducting electrodes overlap within the insulating barrier. This could be compared to bonds between two atoms forming a molecule. As for a molecule one can define the so called binding energy. It is also possible to define the Josephson coupling energy for a Josephson junction. This Josephson coupling energy denotes the energy stored within a Josephson junction and could be calculated by integrating the power over time:

$$E_J(\Theta) = \int_0^{t_0} I_S V \, dt = \frac{\Phi_0 I_0}{2\pi} (1 - \cos(\Theta)). \quad (10)$$

Due to the fact that the integral in equation 10 contains the super current I_S the Josephson coupling energy also depends on the phase difference between the superconducting electrodes. The total potential energy or Gibbs energy of a Josephson junction is than composed of the intrinsic energy of the junction and the applied force multiplied with a generalized coordinate:

$$E_{\text{pot}}(\Theta) = E - Fx. \quad (11)$$

In the case of a Josephson junction the latter part of equation 11 is meant to be the energy that is added or subtracted by applying an external current to the junction. Therefore, the force F can be identified with the externally applied current I and the generalized coordinate x has to be the integral of the voltage drop across the junction. The intrinsic energy of a Josephson junction is given by the Josephson coupling energy. Inserting this into equation 11 the potential energy of a Josephson junction is given by

$$E_{\text{pot}}(\Theta) = E_J(\Theta) - I \left(\frac{\Phi_0}{2\pi} \Theta + c \right). \quad (12)$$

The potential energy is shown in figure 6 for two different values of the externally applied current I .

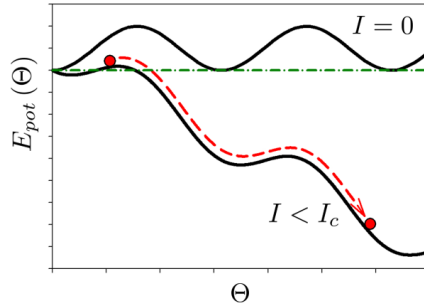


Figure 6: Potential energy of a Josephson junction for an externally applied current $I = 0$ and $I < I_C$ [8].

For the case of $I = 0$ the potential energy is oscillating sinusoidal around a certain value of E_{pot} , displayed in figure 6 by the upper curve. For currents that are unequal to zero, the potential energy becomes phase dependent as displayed in the second curve in figure 6. Depending on the value of I , the potential is tilted by a certain angle. Due to this tilting, the shape is called tilted washboard potential. As long as the externally applied current is below the critical current I_0 there are still potential minima, but if I becomes larger than I_0 all minima vanish and an imaginary phase particle sitting in the potential could freely move downwards to lower energy [3, 8].

2.1.4 Voltage State of a Josephson junction

The Josephson junction described so far was regarded to be in a zero voltage state, meaning that all current I flows as Cooper pairs through the junction. The mode of a Josephson junction, that is described in the following differs, as the externally applied current I is larger than the critical current I_C . In this situation only a part of the current I is carried by Cooper pairs. Therefore the total current I flowing through the Josephson junction is given by

$$I = I_S + I_N + I_D + I_F. \quad (13)$$

The components, apart from the super current I_S of equation 13 are explained in the following.

Normal Current I_N The normal current I_N flowing through a Josephson junction can, in general, be described by Ohm's law:

$$I_N = G_N V, \quad (14)$$

where G_N stands for the normal conductance of the Josephson junction. In general the normal conductance of a Josephson junction depends on the temperature of the junction as well as the voltage drop across the junction:

$$G_N = G_N(V, T) \quad (15)$$

Talking about the value of the normal conductance G_N four cases must be discussed:

1. For temperatures T close to the critical temperature T_C of the junction, i.e. $T \leq T_C$, the required energy to break a Cooper pair is much smaller than the thermal energy $k_B T$. Therefore almost all Cooper pairs are broken up and the concentration of quasi-particles is close to the density of electrons in the normal conducting state. In this state the resistance of the Josephson junction is close to the normal state resistance

$$I_N = G_N V \quad \text{with} \quad G_N = \frac{1}{R_N} \quad (16)$$

2. If the voltage across the Josephson junction is higher than gap voltage V_g of the Josephson junction, the external current source (electrical current) provides sufficient energy eV to break up Cooper pairs. In this case a Cooper pair is broken up in one of the electrodes creating a quasi-particle that passes to the other electrode. This results in the fact that the current voltage characteristic is approaching the temperature independent behavior of the normal conducting state:

$$I_N = G_N V \quad \text{with} \quad G_N = \frac{1}{R_N} \quad (17)$$

3. For temperatures $T \ll T_c$ and voltages $|V| < V_g$, neither the thermal energy $k_b T$, nor the electric energy eV is sufficient to externally break up Cooper pairs. Therefore the normal current is vanishing small:

$$I_N = G_N V = 0 \quad \text{with} \quad G_N = 0. \quad (18)$$

4. At a finite temperature of $T > 0$, there is a finite number of quasi-particle in the superconducting electrode due to thermally broken Cooper pairs, which can already tunnel through the barrier at voltages smaller than the gap voltage. This results in a finite resistance, the so called subgap resistance R_{sg} . This subgap resistance is determined by the number of thermally broken Cooper pairs and the normal current is given by

$$I_N = G_N V \quad \text{with} \quad G_N = G_{sg}. \quad (19)$$

Summarized, the normal current of a Josephson junction is described by a voltage and temperature dependent conductance $G_N(V, T)$:

$$\frac{1}{R_{sg}(T)} \quad \text{for} \quad |V| < V_g \quad (20)$$

$$\frac{1}{R_N} \quad \text{for} \quad |V| \geq V_g. \quad (21)$$

In figure 7 the current-voltage characteristic, following from these two values of the normal conductance of a Josephson junction, is displayed:

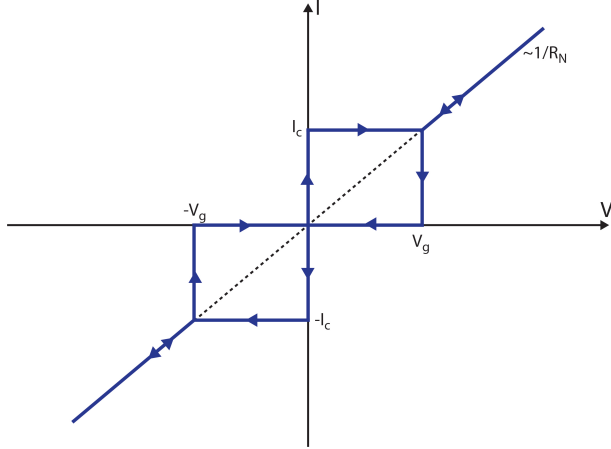


Figure 7: Current-voltage characteristic of a Josephson junction. This drawing of a current-voltage characteristic assumes very low temperatures leading to a vanishing subgap resistance.

Displacement Current I_D From outside, a Josephson junction looks like a plate capacitor and therefore has a finite capacitance C . Hence, the displacement current has to be taken into account for situations where the voltage V across the junction is changing with time ($dV/dt \neq 0$). In this situation it is given by

$$I_D = C \frac{dV}{dt}. \quad (22)$$

Fluctuation Current I_F The Brownian motion of quasiparticles within the Josephson junction causes a current noise that can be expressed according to Nyquist's theorem as

$$S_J(f) = \frac{4k_B T}{R_N} \quad (23)$$

This fluctuation current is temperature dependent and influences the behavior of the Josephson junction.

Equivalent circuit of a Josephson junction and junction equation According to the discussion of the current contributions within a Josephson junction it is possible to draw the equivalent circuit displayed in figure 8.

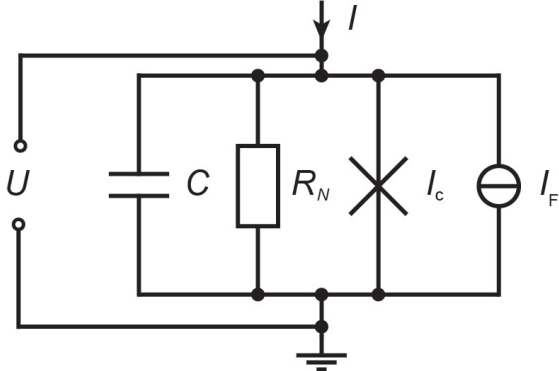


Figure 8: Equivalent circuit of a Josephson junction. As described above the total current I is composed out of four different components [6].

Using the given relations for the current contributions it is possible to set up the so called basic junction equation:

$$I = I_C \sin(\phi) + G_N(V)V + C \frac{dV}{dt} + I_F. \quad (24)$$

2.1.5 Josephson junction in magnetic fields

Until this point a Josephson junction was assumed to be a point-like object, but as they are real life objects they are not point-like at all. The area of a Josephson junction is defined by the contact area of the superconductor-insulator-superconductor area. Thus, it has to be taken into consideration that the phase difference Θ is changing with the position within the tunnel barrier.

To analyze the dependency of the critical current I_C of the external magnetic field B , one can observe the phase change along a closed integration path. This is schematically displayed in the inset of figure 9.

As the macroscopic wave function has to be well-defined, a change of phase along the integration path is displayed by the inset of figure 9 can only be integer multiples of 2π . The phase difference between the points z_1 and z_2 is given by

$$\phi(z_2) - \phi(z_1) = \frac{2\pi\Phi}{\Phi_0}. \quad (25)$$

By making the distance $dz = z_2 - z_1$ infinitesimal small, integrating equation (25) and inserting the result in the first Josephson equation (5) results in a position dependent super current density:

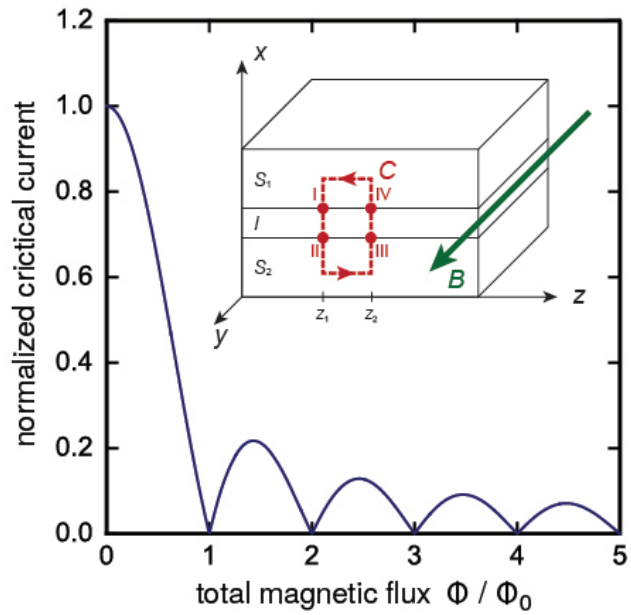


Figure 9: Normalized critical current of a Josephson junction, depending on the magnetic flux inside the SQUID loop [6]. Inset: Josephson junction, penetrated by a magnetic field. The red line indicates a closed integration path.

$$j_S(z) = j_C \sin \left(\frac{2\pi}{\Phi_0} B z d^* + \phi_0 \right) \quad (26)$$

Here, B denotes the magnetic field density and d^* denotes the effective thickness of the barrier. Integrating this super current density across the whole junction area, shows that the critical current of the Josephson junction depends on the magnetic flux within the junction:

$$I_S^{\max}(\Phi) = I_C \left| \frac{\sin(\pi\Phi/\Phi_0)}{(\pi\Phi/\Phi_0)} \right|. \quad (27)$$

This relation between the maximum super current and the magnetic flux inside the junction is shown in figure 9, were the normalized critical current is plotted as a function of the magnetic flux inside the Josephson junction. This feature of a field dependent critical current of a Josephson junction is exploited by the design of Superconducting Quantum Inference Devices. These devices are discussed in the following.

2.1.6 dc-SQUIDs

Within figure 10 a schematic drawing of a so called direct-current Superconducting Quantum Interference Device (dc-SQUID) is displayed. The simplest picture of a dc-SQUID is a superconducting loop that is separated by two Josephson junctions symbolized by crosses. In parallel to these two Josephson junctions, there are two shunt resistors, necessary to prevent the SQUID from hysteretic behavior.

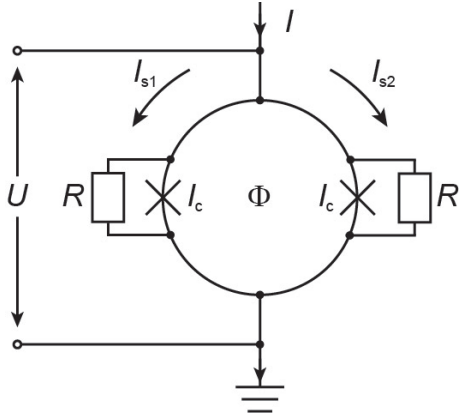


Figure 10: Schematic drawing of a dc-SQUID [6]. The superconducting loop is interrupted by two Josephson junctions indicated by crosses. In parallel to these Josephson junctions shunt resistors prevent hysteretic behavior of the SQUID.

Both Josephson junctions within figure 10 are assumed to be identical, thus the current phase relations $I_{s1} = I_C \sin(\phi_1)$ and $I_{s2} = I_C \sin(\phi_2)$ hold. From Kirchhoff's second law follows:

$$\begin{aligned} I_S &= I_C \sin(\phi_1) + I_C \sin(\phi_2) \\ &= 2I_C \cos\left(\frac{\phi_1 - \phi_2}{2}\right) \sin\left(\frac{\phi_1 + \phi_2}{2}\right). \end{aligned} \quad (28)$$

By integrating equation (28) along the SQUID loop it can be shown, that the phase difference $\phi_1 - \phi_2$ is proportional to the magnetic flux Φ inside the SQUID loop and given by $\phi_1 - \phi_2 = 2\pi\Phi/\Phi_0$. Inserting this into equation (28) results in the super current

$$I_S = 2I_C \cos\left(\pi\frac{\Phi}{\Phi_0}\right) \sin\left(\phi_1 + \pi\frac{\Phi}{\Phi_0}\right) \quad (29)$$

Equation (29) together with the fact that the total flux within the SQUID loop is given by $\Phi = \Phi_{\text{ext}} + LI_{\text{circ}}$ results in an equation for the total flux within the SQUID loop to be

$$\Phi = \Phi_{\text{ext}} - LI_c \sin\left(\frac{\phi_1 - \phi_2}{2}\right) \cos\left(\phi_1 + \pi\frac{\Phi}{\Phi_0}\right) \quad (30)$$

Here, L stands for the inductance of the SQUID loop and $I_{\text{circ}} = (I_{s1} - I_{s2})/2$ is the shielding current inside the SQUID loop.

According to equation (28), $\sin(\phi_1) \approx -\sin(\phi_2)$ holds for small currents $I_S \ll I_C$. Inserting this into equation (30) results in

$$\begin{aligned} \Phi_{\text{ext}} &= \Phi + LI_C \sin\left(\frac{\phi_1 - \phi_2}{2}\right) \\ &= \Phi + \frac{\Phi_0\beta_l}{2} \sin\left(\frac{\phi_1 - \phi_2}{2}\right), \end{aligned} \quad (31)$$

which is a relation between the externally applied flux and the total flux inside the SQUID loop. In this equation β_l is defined as

$$\beta_l = \frac{2LI_c}{\Phi_0}, \quad (32)$$

which is called shielding factor. It gives the relation between the maximum shielding current $I_{\text{circ}}^{\max} = I_C$ and $\Phi_0/2$. Within figure 11 the total magnetic flux within the SQUID loop is plotted against the externally applied magnetic flux. It is obvious that for $\beta_l > 2/\pi$ the curve becomes ambiguous. In the case that the external flux is equal to $n\Phi_0$ the circular current becomes zero and the total magnetic field is equal to the externally applied one, which is displayed as the nodes in figure 11.

The fact that for externally applied fluxes equal to $n\Phi_0$ no additional flux is induced by shielding currents within the SQUID loop, results in an unchanged critical current of the Josephson junctions of the SQUID. Therefore, the current I, which is smaller than $2I_C$ of the single junction and applied for the operation of the SQUID is completely carried by Cooper Pairs through the Josephson junctions. This results in a vanishing voltage drop across the SQUID for $\Phi_{\text{ext}} = n\Phi_0$.

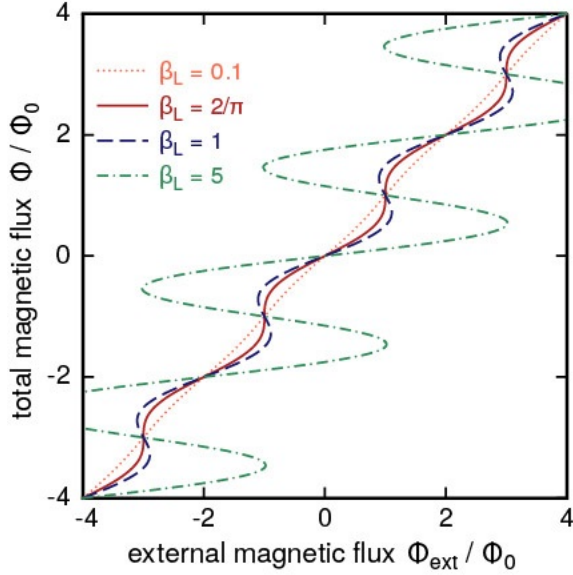


Figure 11: The total magnetic flux Φ/Φ_0 in dependency of the externally applied magnetic flux Φ_{ext}/Φ_0 for different values of β_L [6].

2.2 Noise Thermometers

Noise thermometers are the only type of thermometers which can cover the full temperature range of solids from thousands of kelvin to micro-kelvin. The variants of those noise thermometers used in low and even ultra-low temperature applications cover a wide range of temperature, with a single device. This range starts, depending on details of the device, at temperatures of a few kelvin and reaches down to several micro-kelvin, hence they cover several orders of magnitude within the temperature scale.

But the most important fact about them is that the measured quantity is based on a fundamental physical relation, which allows noise thermometers to be used as primary thermometers. In general, as the name already suggests, noise thermometers use the noise of a physical quantity to determine the temperature. More specific, the thermometers discussed during this lab course use the thermal noise of electrons within an electrical conductor. This thermal noise is a result of the Brownian motion of the electrons within the conductor and its amplitude can be described by the so-called Nyquist formula [11]. In contrast to the measurement of the thermal voltage noise across a resistor at high temperature, the same at low and ultra low temperatures comes along with some experimental challenges. These challenges arise from the fact that the voltage fluctuations across a resistor become smaller and smaller with decreasing temperature. This decreasing signal requires an amplifier with a very low intrinsic noise. As already discussed in the previous section so called superconducting quantum interference devices (SQUIDs) fulfill those requirements. During this lab course noise thermometers are explained and used as one possible application of the described SQUIDs.

2.2.1 Thermal Noise

In the year of 1827, Robert Brown published his observations on pollen suspended in water [2]. He observed that these particles randomly move around the liquid. In the following years, this random motion of particles was called Brownian motion. Later the observations of Brown were explained in a theoretical way by Albert Einstein [4], being a thermal motion of these particles. Similar to particles suspended in liquids, also electrons within a conductor show the behavior of thermal motion. The later phenomenon was initially discovered by John B. Johnson [9]. In the following, the thermal motion of electrons within a conductor is called thermal noise or simply noise. In [10] Johnson showed, that in a given bandwidth Δf , the variance $\langle U^2 \rangle$ of the voltage across an electrical resistor is proportional to the temperature T and the value R of the resistor. Shortly after this discovery Harry Nyquist identified the thermal motion of charge carriers inside a metal as the reason for this behavior [11]. For the relation between temperature, resistance, and voltage variance he derived

$$\langle U^2 \rangle = 4k_B T R \Delta f, \quad (33)$$

which is often called Nyquist formula.

To sketch how this relation can be derived, we follow a thought experiment made by Nyquist [11]. We begin with two electrical resistors $R_1 = R_2 = R$ connected to each other as drawn in figure 12. The thermal motion of the charge carriers in resistor R_1 leads to a voltage drop δU_1 across it. This voltage drop drives a current $I_2 = \delta U_1 / (R_2 + R_1)$ through the resistor R_2 . Similarly, a voltage fluctuation δU_2 across the second resistor drives a current $I_1 = \delta U_2 / (R_1 + R_2)$ through resistor R_1 .

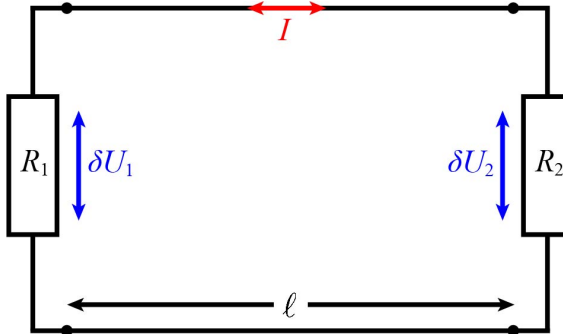


Figure 12: Electrical circuit of Nyquist's thought experiment [12]. The two resistors R_1 and R_2 are in thermal equilibrium at temperature T and are connected via a transition line of length ℓ . For the values of the resistors we assume $R_1 = R_2 = R$.

As mentioned above the resistors R_1 and R_2 are equal, therefore the voltages δU_1 and δU_2 are equal and can be replaced by δU . Due to the equality of the voltages across both resistors, also the current flowing through both resistors is equal to $I = \delta U / 2R$. This current leads to power dissipation of

$$P = \langle I^2 \rangle R = \frac{\langle \delta U^2 \rangle}{4R} \quad (34)$$

in each resistor. Using the second law of thermodynamics, Nyquist concluded that the power transferred from R_1 to R_2 is equal to the power transferred in the reverse direction, from R_2 and R_1 . It is worth to notice, that all assumptions made so far do not limit the choice of material for the resistors. It is possible to imagine metallic, electrolytic, or any other conducting material in this thought experiment. Equation 34 must hold for every frequency band Δf , but in the general case the resistance of the resistor might depend on frequency, $R = R(f)$, making equation 34 frequency dependent. This leads to the conclusion that the function describing the voltage drop across the resistors due to the thermal motion of the charge carriers is a function of resistance, temperature and frequency.

The function describing the voltage drop can be determined by looking at the energy that is traversing the lines between the resistors. Let us imagine an amount of energy δE , emitted from R_1 , traversing from R_1 to R_2 and absorbed by the resistor R_2 . The same amount of energy must also traverse in the opposite direction being emitted by R_2 and absorbed by R_1 . This flow of energy can be imagined as a superposition of waves, moving with a speed of $v = \partial\omega/\partial k = \omega/k$ through the transmission line. These waves can be described by

$$U(x, t) = U_0 e^{i(kx - \omega t)}. \quad (35)$$

Within this equation, ω represents the angular frequency, k the wave number, and U_0 a voltage amplitude. At any time after the thermal equilibrium is reached, the transmission line is detached from both resistors simultaneously. After this separation the propagating waves will get reflected at both ends of the transmission line, hence the energy emitted by the resistors is now trapped inside the transmission line. We now connect the ends of the transmission line and describe the propagating waves by the complete basis of functions, that is given by sinusoidal waves $U \sin(\omega t - ka)$ that fulfill periodic boundary conditions, $kl = 2\pi n$, and propagate left or right. In the further course it is sufficient to consider one of the resistors and one direction of propagation of the voltage wave. For the number N of allowed modes within a certain frequency band between ω and $\omega + \Delta\omega$ we find

$$N = \ell \frac{\Delta k}{2\pi} = \frac{\ell}{v} \frac{\Delta\omega}{2\pi}. \quad (36)$$

Each of those modes was in thermal equilibrium with the resistor before we detached the lines. Therefore, its occupation is given by the Bose-Einstein distribution and we find for the energy carried by this mode

$$E(\omega) = \frac{\hbar\omega}{e^{\hbar\omega/k_B T} - 1}. \quad (37)$$

Within this formula \hbar represents the reduced Planck constant, k_B the Boltzmann constant and T the temperature of the system. In the case of $\hbar\omega \ll k_B T$ equation 37 simplifies to

$$E = k_B T. \quad (38)$$

This equation is describing the classical limit. The thermal power each of the two resistors is emitting into each mode can be calculated by dividing the energy E by the time t it took to emit the corresponding wave into the transmission line. In the case of this experiment this time $t = l/v$ is defined by the length ℓ of the conduction lines and the speed v of the waves traversing through the lines. As the power transmitted by one mode is $P = E/t$ we find for the power transmitted by the $N = \Delta f l/v$ modes within a frequency band Δf

$$\frac{P(f)}{\Delta f} = \frac{N}{\Delta f} \frac{E}{t} = k_B T \quad (39)$$

By inserting equation 34 into equation 39, and solving for the variance of the voltage, we find the known Nyquist formula:

$$\langle U^2 \rangle = 4k_B T R \Delta f. \quad (40)$$

Note that there was no assumption on the nature of the resistors made. Therefore, the Nyquist formula holds not only for ohmic resistances but also for every kind of dissipative component. Taking this into account the resistance R within equation 40 can be replaced by a complex and frequency dependent impedance $Z(f)$. However, as the application of noise thermometry deals with an ohmic resistance, the Nyquist formula will be used as it is written within equation 40 in the following.

2.2.2 Principle of noise thermometry

As already mentioned the noise thermometers make use of the fundamental physical property of thermal noise to measure the temperature. The kind of noise thermometer used within this lab course is a very simple one, whose setup is described in chapter 4. For this part of the introduction it is sufficient to know that the thermal noise exhibited by a resistor is measured using a two stage SQUID setup as described in section 3.3 and that the resistor is connected in serial to the input coil L_{in} of the single SQUID frontend. This serial connection of the resistor and L_{in} is symbolized by the circuit shown in figure 13. The thermal noise $\langle U^2 \rangle$ exhibited by the resistor R is symbolized by the voltage source U as the resistor and the inductance within the circuit in figure 13 are assumed to be ideal. It is obvious that the circuit shown in figure 13 shows a low pass like behavior, as the serial connection of a resistor and an inductance is the simplest form of a low pass. This leads to a frequency dependency of the current measured with the ampere meter. Thus, it is necessary to consider every single frequency bin of the measured signal. The easiest way to do so is calculating the Fourier-transform of the measured signal, resulting in the so called power spectral density. The way to calculate the same for the circuit displayed in figure 13 is shown in the following.

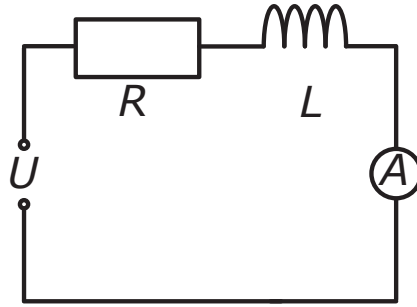


Figure 13: Equivalent circuit of the input circuit used for the discussed noise thermometers.

The schematic drawing consists of a resistance R , an inductance L , a voltage source U , and an ampere meter. The combination of R and L leads to a low pass like behavior of the circuit.

Power spectral density of the RL circuit Every dissipative component of an electric circuit is in general frequency dependent, therefore the power spectral density is also frequency dependent. This is because the power spectral density describes the power contained within a certain frequency band Δf . The power spectral density $S_A(f)$ of a quantity A satisfies the equation

$$\int_{f_0}^{f_0+\Delta f} S_A(f) df = \langle A^2 \rangle. \quad (41)$$

The $\langle A^2 \rangle$ within equation 41 describes the variance of the measured parameter within a frequency band $[f_0, f_0 + \Delta f]$. Due to this equation the unit of the power spectral density depends only on the unit of the measured quantity A . For the voltage fluctuations described by the Nyquist formula, equation 40, above we find the power spectral density

$$S_U = \frac{\langle \delta U^2 \rangle}{\Delta f} = 4k_B T R. \quad (42)$$

In this case, the unit of the power spectral density is $V^2 \text{Hz}^{-1}$. In literature and publications sometimes the terms noise power, noise spectrum, or noise are used as synonym for the power spectral density (PSD). Often also, the square root of the PSD is considered, which has the unit $V/\sqrt{\text{Hz}}$. According to Kirchhoff's law, the circuit representing the noise thermometers discussed within this lab course and shown in figure 13 is described by

$$U - RI - i\omega LI = 0, \quad (43)$$

where ω represents the angular frequency of the alternating voltage U generated by the voltage source. Rearranging equation 43 and introducing the cutoff frequency $f_c = R/2\pi L$ we find for the ratio of voltage and current amplitudes

$$\frac{|U|}{|I|} = R \sqrt{1 + \frac{f^2}{f_c^2}}. \quad (44)$$

Analogous to the power spectral density of a voltage, as it is given by equation 42, the power spectral density for the current is given by

$$S_I = \frac{|I^2|}{\Delta f} = S_U \frac{|I|^2}{|U|^2}. \quad (45)$$

By inserting equation 42 and equation 44 the current power spectral density for the circuit displayed in figure 13 is given by

$$S_I(f) = \frac{4k_B T}{R} \frac{1}{1 + \frac{f^2}{f_c^2}} \quad (46)$$

which is given in units of $\text{A}^2 \text{Hz}^{-1}$

The first factor within equation 46 results in a constant value, which is determined by the resistance R and the temperature T of the system. Whereas the second factor is describing the frequency dependence, i.e. the low pass like behavior of the circuit. The spectral shape is only determined by the cutoff frequency $f_c = R/2\pi L$. This frequency denotes the frequency at which the amplitude of the signal has dropped to $1/\sqrt{2}$ times its original value and can be changed by changing the resistance R or the inductance L of the circuit. Using equation 46 it is possible to calculate the shape of the power spectral densities for the circuit displayed in figure 13. Figure 14 shows the current noise for fixed R and L at different temperatures on the left side as well as for fixed L and T , but different resistances on the right side.

Having a look at the left plot in figure 14, where the resistance and inductance are kept constant at $R = 5 \mu\Omega$ and $L = 5 \text{nH}$ the amplitude of the spectra increases with increasing temperature. With these values for the resistance and the inductance the cutoff frequency takes the value $f_g \approx 160 \text{ Hz}$. In contrast, for the right plot of figure 14 the temperature and the inductance are kept constant at $T = 10 \text{ mK}$ and $L = 5 \text{nH}$ and the resistance is varied. The resistance values shown in this plot are typical values used for state of the art noise thermometers. From the plot it is visible that with increasing resistance, the cutoff is shifted towards higher frequencies and the value of the plateau is reduced [5, 7, 1, 12].

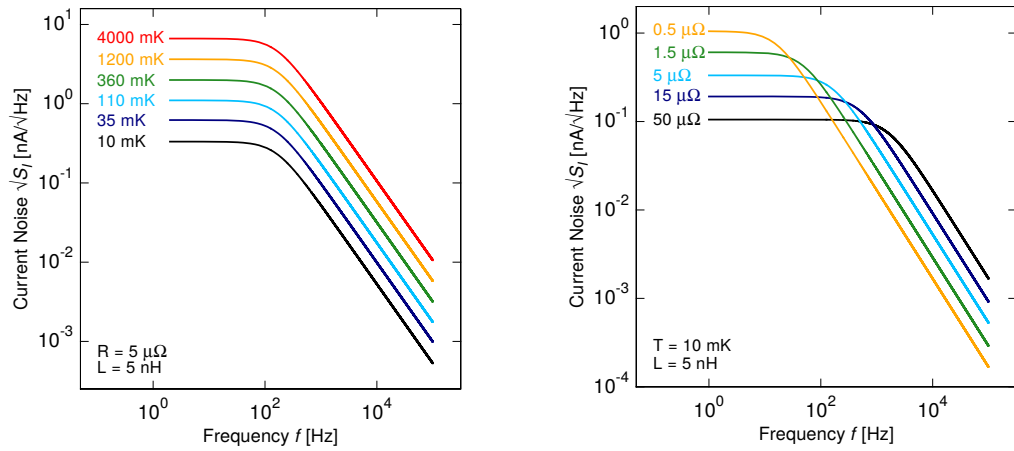


Figure 14: Current noise of a circuit composed out of a resistor R and an inductance L at a temperature T [12]. The spectra are calculated using equation 46. Left: The resistance and the inductance are kept constant at $R = 5 \mu\Omega$ and $L = 5 \text{nH}$, only the temperature is varied. Right: The temperature and inductance are kept constant at $T = 10 \text{ mK}$ and $L = 5 \text{nH}$ and the resistance is varied.

3 Methods

In this chapter the basic concepts of SQUIDs as sensitive magnetometers are discussed. This includes the linearization of the output signal via flux-locked-loop and low-noise two-stage SQUID setups. How the thermal noise of a resistor can be used to calculate its temperature is explained at the end.

3.1 dc-SQUID Characteristics

A technical drawing of a dc-SQUID circuit as it will be used within circuits later can be seen in figure 15. Here, the Josephson junctions drawn are shunted, non-ideal junctions and can be described by the RCSJ model.

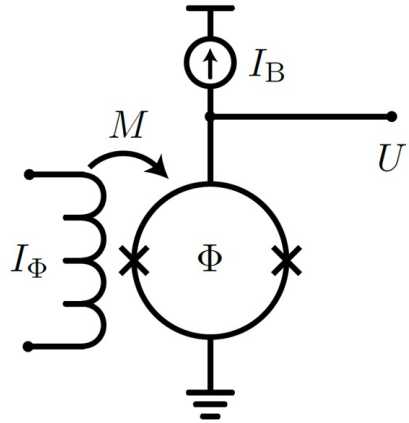


Figure 15: Simple circuit containing a dc-SQUID operated at the constant bias current I_B [13]. The voltage drop U across the SQUID depends on the magnetic flux Φ inside the SQUID and the bias current I_B . A flux change $\Delta\Phi$ can be generated by the current I_Φ in a superconducting coil, coupled to the SQUID via the mutual inductance M .

Such a SQUID is usually operated with a constant bias current I_B . For small bias currents, the Cooper pairs of the superconductors can tunnel through the Josephson junctions without dissipation and thus no voltage drop occurs. At higher bias currents above a critical current I_C , Cooper pairs break up and tunnel as quasi-particles through the junctions and create a voltage drop U over the SQUID. The critical current I_C depends periodically on the magnetic flux Φ inside the SQUID where the period is given by the magnetic flux quantum Φ_0 . Thus, the voltage drop U over the SQUID is a function of the bias current I_B and the magnetic flux Φ . A change of magnetic flux $\Delta\Phi$ can be generated by a superconducting coil coupled to the SQUID. The flux change inside the SQUID is given by

$$\Delta\Phi = I_\Phi M, \quad (47)$$

where I_Φ is the current through the coil and M is its mutual inductance. The current-voltage characteristic, which is the voltage drop U over the SQUID as a function of the bias current I_B , is shown in figure 16 on the left-hand side for integer as well as half-integer flux quanta inside the SQUID loop. For any other flux value the output lies in between the two curves. At a given bias current the voltage has a maximum at half-integer magnetic flux quanta and a minimum at integer flux quanta. The bias current I_B is marked where the voltage swing is maximal. The corresponding voltage as a function of the magnetic flux in the SQUID is shown in figure 16 on the right-hand side. The flux-voltage characteristic can be used to calculate the mutual inductance M of the superconducting coil to the SQUID using the equation 47. Here, this was already done to convert the current through the superconducting coil to a flux in units of magnetic flux quanta. For our SQUIDs, we usually determine the inverse mutual inductance M^{-1} and provide it in units of $\mu\text{A } \Phi_0^{-1}$. The current-voltage and flux-voltage characteristics shown in figure 16 were obtained during a characterization of a SQUID produced in our cleanroom. The maximal voltage swing was found using $I_B = 14.6 \mu\text{A}$ and $M^{-1} = 42(1) \mu\text{A } \Phi_0^{-1}$ was measured. The characterization was performed at 4.2 K in a helium can.

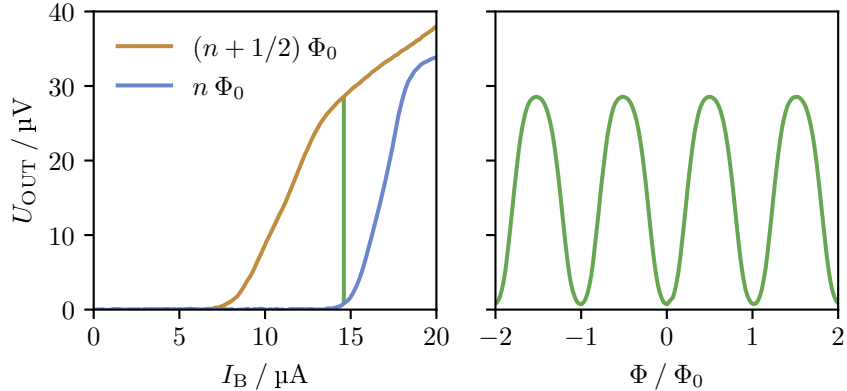


Figure 16: Current-voltage and flux-voltage characteristics [13]. The voltage drop over the SQUID is shown on the left hand side for half-integer and integer flux quanta. On the right hand side the voltage is shown as a function of the flux inside the squid.

A SQUID can be operated as a sensitive magnetometer as its output voltage depends strongly on the magnetic flux. For the SQUID mentioned above, the bias current with the highest voltage swing and a magnetic flux of $1/4 \Phi_0$ was used to measure an amplification of $109 \mu\text{V } \Phi_0^{-1}$ which is the slope at the inflection point of the flux-voltage characteristic shown in figure 16 on the right-hand side. This specific magnetic flux and bias current were used since the slope of the voltage-flux characteristic is maximal in this case. However, a SQUID alone is not suited as a flux to voltage converter for practical purposes. Due to it

periodicity of its voltage-flux characteristic, the output voltage is not unique as several input flux values can lead to the same output voltage.

3.2 Flux-Locked-Loop

The signal of a SQUID can be linearized by a flux-locked loop (FLL) setup. A schematic drawing of an FLL circuit is shown in figure 17. To achieve a well defined magnetometer, the output voltage U_{OUT} is used to produce a negative flux feedback in the SQUID via the feedback coil and the resistance R_F . The closed loop will counteract a flux change in the SQUID such that the voltage drop over the SQUID is zero and hence the integrator does no longer change the output voltage. A flux change from the input coil will be compensated by a corresponding negative flux change from the feedback coil.

The counteracting flux changes are given by

$$\Delta\Phi = \Delta\Phi_{\text{IN}} + \Delta\Phi_B = 0 = \Delta I_{\text{IN}} M_{\text{IN}} - \Delta I M_{\Phi B} \quad (48)$$

where I is the current through the feedback coil. Using the output voltage, one finds

$$\Delta I = \frac{\Delta U_{\text{OUT}}}{R_F} \quad (49)$$

which can be further used. Combine and rearranging leads to

$$\Delta U_{\text{OUT}} = -R_F \frac{M_{\text{IN}}}{M_{\Phi B}} \Delta I_{\text{IN}} \quad (50)$$

for the output voltage which is thus proportional to the input current. The amplification factor is given by $R_F M_{\text{IN}} / M_{\Phi B}$ and hence is an effective resistance.

The feedback will lead to a fixed working point of the SQUID that is set by I_B , $I_{\Phi B}$ and U_B . At the given biases, the working point is then defined by the flux at which the voltage drop over the SQUID is zero. To reach a good signal to noise ratio, a working point with a strong flux dependence is favored.

The described circuit can be used to acquire the change of flux produced by a current I_{IN} through the input coil, but it has some limitations. It is important to note that positive feedback could occur due to a lag of the feedback and thus a phase difference between signal and feedback might occur. The feedback could then be positive. This has to be excluded by a well tuned integrator which is realized by a low-pass filter. In the case of positive feedback, a lower cut off frequency of the integrator is necessary even though this leads to a reduced bandwidth. Also, the feedback circuit can potentially be too slow to regulate the flux compensation of a fast and large flux change. This can result in a jump of the working point of multiple integer flux quanta in the flux-voltage characteristic and thus a cropped output signal.

3.3 Two-Stage SQUID-Readout

To decrease the noise and hence increase the signal to noise ratio of the flux-locked loop circuit with a single SQUID, two SQUID stages can be used. A drawing of a two-stage

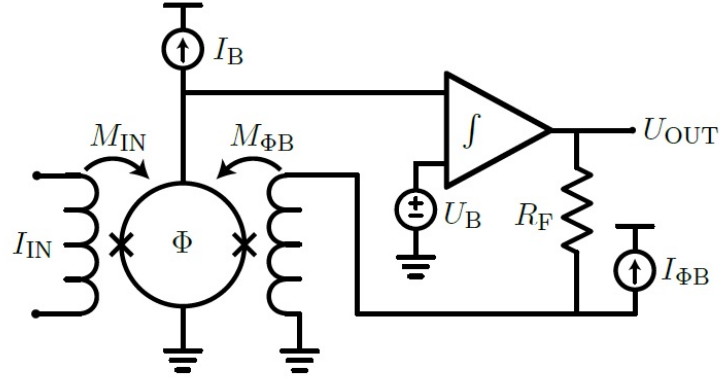


Figure 17: Flux-locked-loop circuit with a single SQUID [13]. A negative feedback is used to linearize the periodic signal of the SQUID.

FLL SQUID circuit can be seen in figure 18. A current change I_{IN} in the input coil creates a flux change $\Delta\Phi_1 = I_{IN}M_{IN}$ in the first stage SQUID, also referred to as frontend SQUID. This configuration allows to operate the first stage SQUID in a voltage bias to reduce the power dissipation of the SQUID. The flux change of the first stage SQUID generates a current change which creates a flux change $\Delta\Phi_2$ in the second stage SQUID via an input coil. The second stage SQUID consist of multiple in series connected SQUIDs to increase its voltage swing and is thus called SQUID array. The voltage signal of the second stage SQUID biased at a constant current is then amplified and integrated with electronics at room temperature resulting in the output voltage U_{OUT} . Hence, I , I_B , $I_{\Phi X}$, $I_{\Phi B}$ and U_B are used to set the working points of the SQUIDs.

The output voltage is thus also given by equation 50 and the only major difference is a step-wise amplification of the signal before the integrator that leads to a reduced noise. Furthermore both SQUID stages should match each other. Assuming the flux dependent current of the first stage is generating a flux change of more than one Φ_0 in the second stage multiple working points with potential different noise exist. If so, this can be prevented by the so called under-tuning of the first stage SQUID where the voltage swing is reduced by a smaller bias current I , though this results in a decreased signal to noise ratio.

3.4 Temperature measurement using a noise thermometer

In section 2.2.2 the noise power spectral density of a simple circuit consisting of a resistor R and inductance L and a current measurement device, is calculated. As such a circuit is used within state of the art noise thermometers the noise power spectral density of this circuit is used to calculate the temperature. To do so there are two possibilities:

- Adapting the expected shape of the noise power spectral densities (equation 46) to the measured power spectral densities.

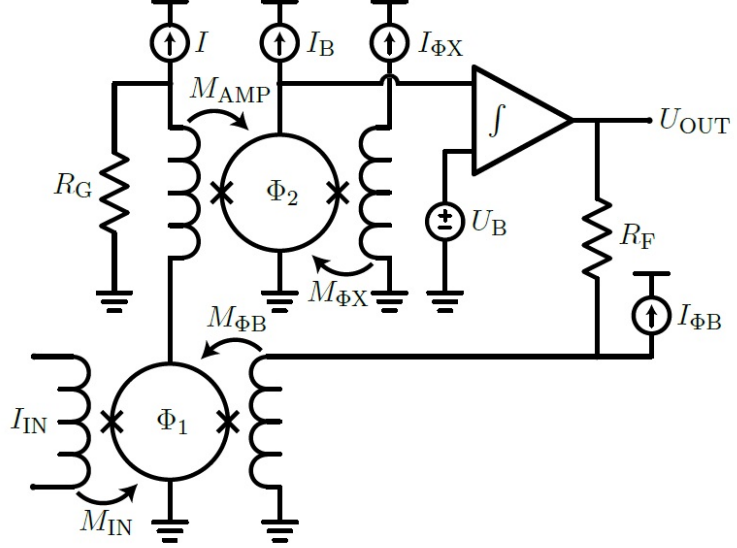


Figure 18: Two-stage SQUID setup using flux-locked-loop readout [13]. The input signal I_{IN} is amplified by two stages before it is integrated and used as a negative feedback.

- Using the linearity in temperature of the noise power spectral densities to make a comparison with a calibration noise power spectral density.

Both methods are used for up-to date noise thermometers and both have their advantages. For the first method, the spectral shape given by equation 46 is adapted to the noise power spectral densities measured with the temperature sensor results in three values: The temperature T , the resistance R of the noise source and the inductance L of the input circuit. The resistance has only one component as the noise source is the only part of the input circuit that is normal conducting, whereas all other components such as the input coil and the wiring are superconducting. However the inductance L has two contributing values, namely the inductance L_{in} of the input coil and the inductance L_{loop} of the input circuit.

In contrast to that the second method makes use of the linear connection between the temperature and the power spectral density measured with the temperature sensor. By dividing the noise power spectral density $S(f)$ by an calibration noise power spectral density $S_{cal}(f)$. By multiplying this quotient with the temperature, the calibration noise power spectral density was recorded at, results in a temperature value that corresponds to $S(f)$. So the temperature is given by

$$T = \frac{S(f)}{S_{cal}(f)} T_{cal}. \quad (51)$$

Due to the experimental setup at a constant temperature, no calibration noise power spectral density is recorded during this lab course, therefore the first method is used to determine the temperature of the liquid helium, the experiment is submerged in.

3.4.1 Uncertainty of the calculated temperatures

In both cases it is possible to determine an uncertainty of the calculated temperature. For the first method of temperature calculation, were the expected spectral shape is adopted to the measured power spectral density, the uncertainty results from the uncertainty of fitting routine.

In contrast to that, the uncertainty of the second way to determine the temperature is only given by the statistical uncertainty of the measured power spectral densities. If it is assumed that the averaging time for the calibration spectrum is very long compared to the single spectra used for temperature calculation, the statistical uncertainty of the calculated temperature is given by

$$\frac{\Delta T}{T} = \left(\frac{1}{t\Delta f} \right)^{\frac{1}{2}}. \quad (52)$$

As this method is not used for the temperature calculation the derivation of this formula is not explained here but in the following section were a state of the art noise thermometer is explained.

4 Setup

Within this section the setup used for this lab course will be explained. At first, the setup of the experiment is explained. Afterwards, you will get an introduction to the functionalities of the software *SQUID Viewer* which allows to control the SQUID electronics and at the end the software of the oscilloscope *PicoScope 6* is described.

4.1 Experimental Setup

Figure 19b shows the setup as it is mounted within a dipstick as shown in figure 19a. The ribbon cable on the right side connects the experiment to the top of the dipstick where the SQUID electronic is connected to the experiment. The used room temperature electronics are capable of reading out up to three independent SQUID setups. However in the case of this lab course only the first two are used. The first channel is connected to a single stage SQUID as drawn in figure 17, whereas the second channel will be used as a noise thermometer and is connected to a two stage setup with a frontend SQUID and a SQUID array as a second stage as drawn in figure 18. The noise source an aluminum wire is connected to the input coil of the frontend SQUID.

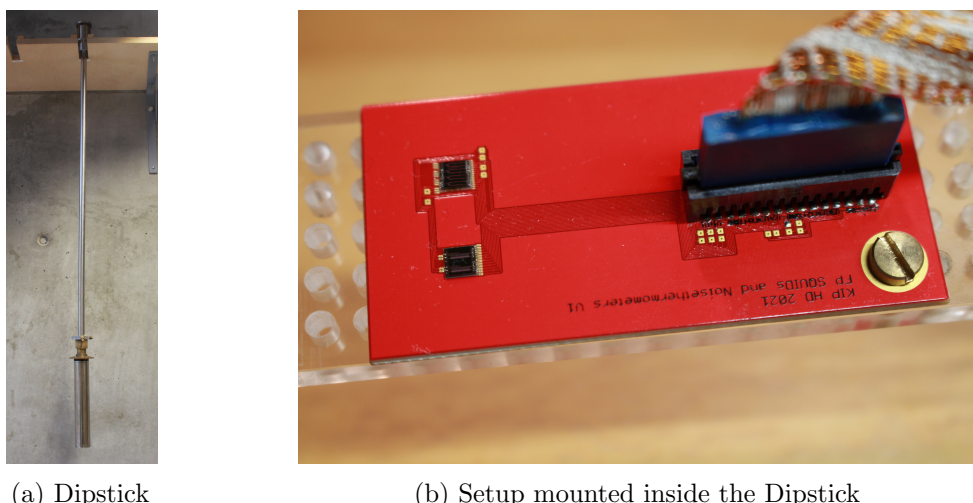


Figure 19: Dipstick with shieldings (a) as well as the experiment mounted inside (b). The dipstick will be put into a ${}^4\text{He}$ transport vessel, with the experiment completely submerged in liquid ${}^4\text{He}$.

For the single stage setup, the feedback and the input coil of the SQUID are connected to the Φ_B and Φ_X channel respectively. Thus it is possible to couple a flux signal to the SQUID loop via both, the input and feedback coil using the respective generator settings within the SQUID viewer. The biasing current for the SQUID itself is applied by using I_B . In the case of the two stage setup, the Φ_X channel is connected to the feedback loop of the SQUID array and the Φ_B channel is used to compensate the flux within the

SQUID loop of the frontend SQUID. The bias current for the frontend SQUID is in this case set by I and the bias current of the array is fed in by Φ_B .



Figure 20: Setup with the dipstick submerged in a liquid ^4He vessel.

The experiment is shielded by a niobium as well as a Cryoperm shield. Both shields reduce external magnetic noise and electric noise. After the shields have been placed over the experiment and fixed with screws, the dipstick is submerged into a ^4He transport vessel. The complete setup is shown in figure 20

4.2 SQUID Viewer

We use the software SQUID Viewer to control the SQUID electronics at room temperature. The most important palettes of the program are shown in figure 21. A palette can be opened by clicking on the respective name with the same color in the main window. The main window (figure 21a) can be used to open the palettes, set the active channel and directly access commonly used functions. The green marked channel (here 22) is the active channel, which means that the information on other palettes refer to this channel. The active channel can be changed by clicking on the respective box of a different channel. Often used functions are e.g. to switch from the amplification mode to the FLL mode or turning generator signals on and off.

The mode palette (figure 21b) is used to switch from the amplification mode to the FLL mode as well as change the feedback resistance in the FLL mode and change the



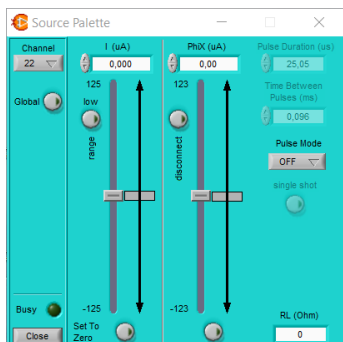
(a) Main window



(b) Mode palette



(c) Bias palette



(d) Source palette



(e) Generator palette

Figure 21: Main Window and the most important palettes of the program SQUID Viewer. The hardware, heater and overload palettes will not be used in this lab course.

gain bandwidth product, which controls the cut-off frequency of the low-pass used for integrating.

The bias palette (figure 21c) and source palette (figure 21d) can be used to set the operating points of the circuit. The labeling is the same as the one introduced in the figures 17 and 18. For tuning the parameters one can either use the rough, fine or ultra fine slider or the input box.

The generator palette (figure 21e) is used to apply alternating signals on the different biases. For this lab course only triangle waveforms with different peak-to-peak values are necessary. The offset 1/2 peak-to-peak has to be activated if one wants to apply a signal that is only positive. Else, a signal going from the negative half peak-to-peak value to the positive half peak-to-peak is generated.

A more in depth description can be found in the manual of the SQUID electronics available during the lab course.

4.3 PicoScope

In the following part, there is an explanation of the basic and necessary functionalities of the oscilloscope software *PicoScope6*. The manual of the software can be found on the manufacturers web page ¹.

In figure 22 the *PicoScope6* software is shown in the oscilloscope mode, with two channels active. The most important buttons are explained with the figure itself. In general the oscilloscope mode is activated by clicking on the scope button, which is marked with a red square.

The line of channel controls, marked with a blue rectangle in figure 22 allows you to change the setting of each input channel independently. The two sliders on the right side of the mode buttons are used to control the timebase of the oscilloscope. These sliders are marked with a blue rectangle. The purple marked slider right beside the timebase controls allows to sweep through the most recent waveforms in the buffer of the oscilloscope. Close to this the zoom buttons are marked with a black rectangle. On the bottom left corner of the displayed graph, two rulers of the time axis are placed. They are indicated by a white square. For each y-axes, two rulers in the corresponding color are placed in either the top right or left corner of the displayed graph. Finally there are the start/stop buttons at the very bottom part of the oscilloscope window, on whose very right side the trigger settings can be found. The latter ones are marked with an orange rectangle. In case you want the software to measure certain parameters like for example frequency or peak-to-peak voltage of the input signals, this could be done with the measurement functions, that are added by clicking on the plus sign close to *Measurements* in the bottom line of the window. This area is marked with a turquoise rectangle.

Figure 23 shows the *PicoScope6* software in the spectrum mode. This mode is activated by clicking on the third button of the mode buttons, which is marked with red square in figure 23.

¹<https://www.picotech.com/download/manuals/picoscope-6-users-guide.pdf>

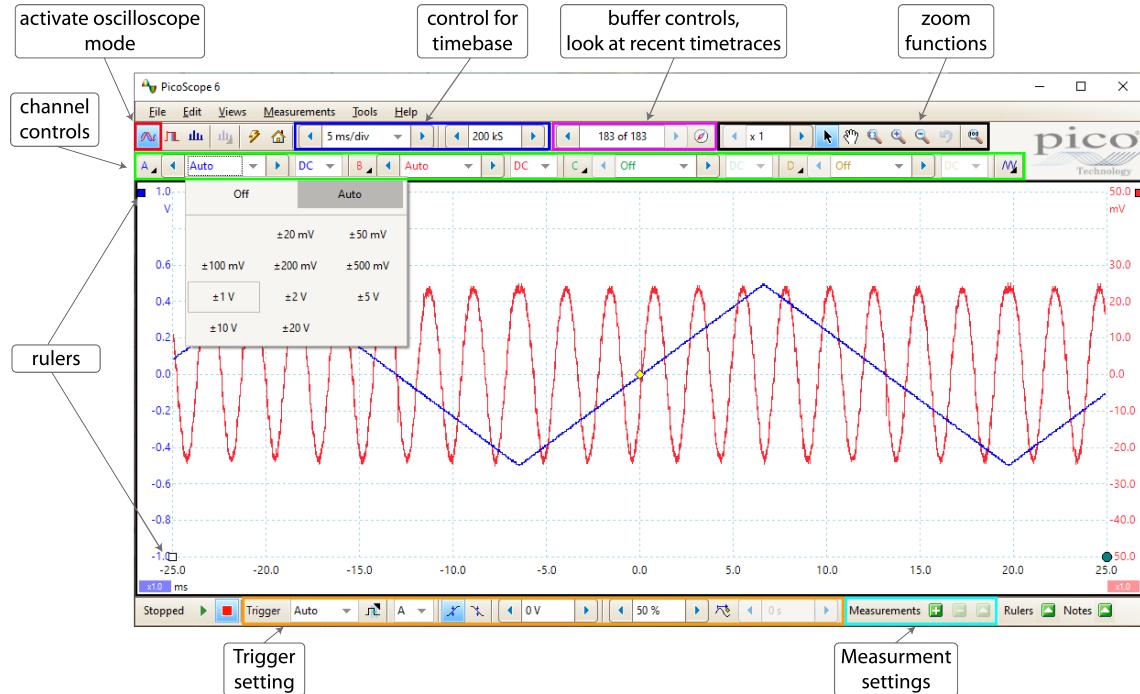


Figure 22: *PicoScope6* software in oscilloscope mode.

By clicking on the button marked with a green square, a window, were you can change the settings of the FFT and the two axes. The frequency bandwidth of the measurement displayed in the graph is shown in a slider right to the settings button. This slider is marked with a blue rectangle and right beside, the slider marked with purple rectangle allows you to sweep through a certain amount of buffered signals. As well as in the oscilloscope mode, there are rulers available in the spectrum mode. These rulers are again placed in lower left corner for the bottom axis (white box) and in the upper right or left corner for the y-axes (colored boxes). At the very bottom left corner of the window there are again the start and stop button for the measurement.

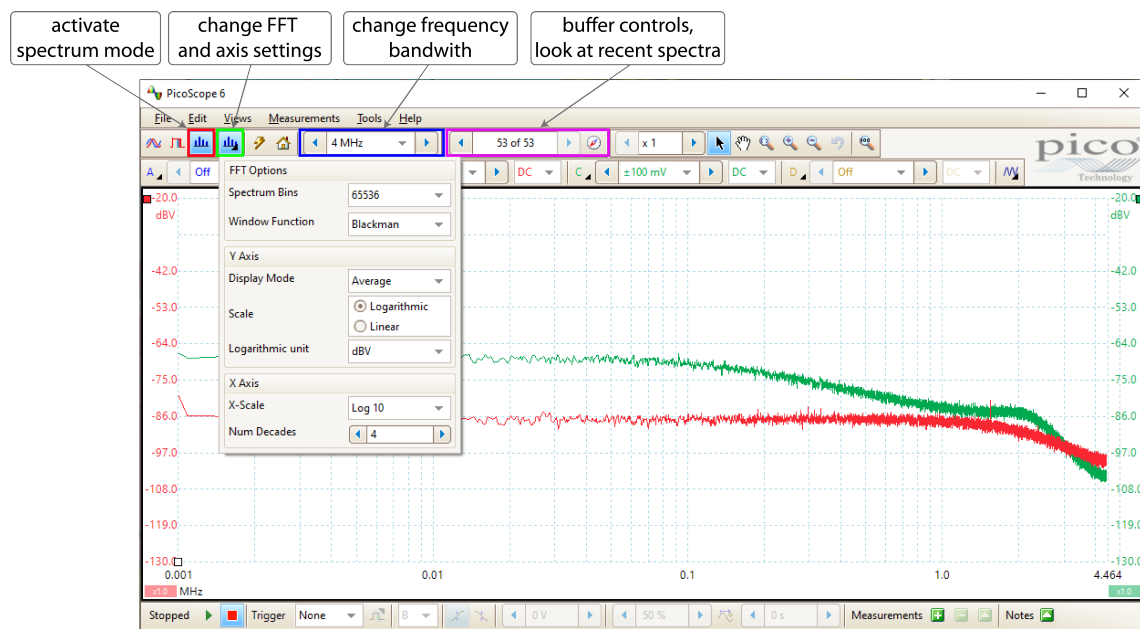


Figure 23: *PicoScope6* in spectrum mode, to display the averaged spectral power density. The settings of the FFT, and the displayed graph can be changed in the shown window.

5 Experiments

This chapter describes the different experiments and provides hints for the completion. At first, make yourself familiar with the setup mounted inside the dipstick and the room temperature electronics. Also, spend some time to learn how the software works once the dipstick is cold. Ask your supervisor if you need help. You will work with liquid helium and expensive state of the art electronics. Cryogenic liquids are dangerous when not handled correctly while the sensitive electronics can break easily when not used with caution. Both, liquid helium and the electronics thus may only be used under supervision. You may play around with the software and conduct experiments on your own once the dipstick is cold and the electronics are connected.

5.1 Preparations

- Measure the resistances of $\pm V$, $\pm \phi$, $\pm \phi_X$, $\pm I$ for both connected channels at room temperature and in liquid helium. Explain the differences and the order of magnitude of the measured resistances.
 - Measure the resistances with the provided multimeter and assume an uncertainty of 1% plus two digits.
 - You may use the auto range of the multimeter at room temperature, but switch to the lowest range if you measure a resistance in liquid helium.
 - What did you measure? How could this measurement be improved?

5.2 Single Stage SQUID

A single SQUID is connected to the first channel. The corresponding circuit for the FLL is figure 18. In AMP mode, the feedback resistance is disconnected and the integrator is replaced by an amplifier.

5.2.1 Open Loop

- **Measurement:** Measure the current-voltage characteristic of the single SQUID in the open loop. Save the current-voltage characteristic for integer and half-integer Φ_0 .
 - In AMP mode, U_{OUT} is amplified by 2000.
 - Use a generator with 1/2 peak-peak offset and set I_B , V_B , Φ_B , I and Φ_X on the bias and source palettes to zero.
 - Set the generator to I_b . The normal conducting resistance should be flux independent. You may set the generator up to the maximal possible value.
 - You may estimate the flux in the SQUID by the shape of the characteristic. (Here a smaller generator signal can be helpful.)

- Take a screenshot of the SQUID viewer windows, you will need the values you adjusted for the generator for the analysis.
- **Analysis:** Plot both current-voltage characteristics with Python. Use the characteristic to determine the resistance of the normal conducting SQUID. What is the resistance of a normal conducting single Josephson junction? Estimate the critical current I_c .
 - Transform your measured data into the right quantities for your final I-V plot.
- **Measurement:** Measure the V-Φ characteristic of the single stage SQUID in the open loop. Note the highest voltage swing V and the corresponding bias current I_B . Save the flux-voltage characteristics for both coils.
 - Apply a generator signal on Φ_B or Φ_X .
 - Increase the bias current I_B to get the flux-voltage characteristic.
 - Find the peak-to-peak voltage at the bias current with the largest voltage swing in μV
 - You can use V_B to center the characteristic around $V_{\text{out}} = 0$
- **Analysis:** Plot the flux-voltage characteristics with Python. Use the characteristics to determine the inverse mutual inductance M_{IN}^{-1} as well as $M_{\Phi B}^{-1}$.
 - The unit of M_{IN}^{-1} and $M_{\Phi B}^{-1}$ is $\mu\text{A } \Phi_0^{-1}$.

5.2.2 Flux Locked Loop

- **Measurement:** Tune the SQUID and activate the FLL mode. Measure the output resulting from the periodic input signal.
 - Tune a single SQUID: Apply a generator on Φ_B . Set I_B to the value with the largest voltage swing and center U_{OUT} with V_B . Turn the generator off and activate the flux-locked-loop mode. Move U_{OUT} with Φ_B to zero.
 - Provide an input signal to the SQUID via Φ_X
 - Is the signal linearised? What influences the amplification? What is the effect of the working point?
 - The working point is set by I_B , V_B , Φ_B .
- **Analysis:** Plot the FLL output resulting from the input signal with Python. Determine the amplification of the circuit in units of $\text{V } \mu\text{A}^{-1}$. Calculate the value one would expect from the measurements before.
 - The expected amplification can be calculated with equation 50

5.2.3 SQUID Noise

- Measure the noise spectrum in FLL mode. Change the gain-bandwidth-product (GBP) and look at the effect on the spectrum.
 - Use the spectrum mode. Set the y and x-scale to logarithmic, the display mode to average and the logarithmic unit to dBV.
 - What is the optimal GBP without resonances?

5.3 Two-stage SQUID Readout

A two-stage SQUID setup is connected to the second channel. The input coil of the first stage SQUID is short circuited with an aluminum wire which functions as a noise thermometer. The corresponding FLL circuit is shown in figure 19.

- **Measurement:** Tune the two-stage SQUID setup. Measure the V - Φ characteristic of the two stage SQUID in the open loop. Note the highest voltage swing V and the corresponding working point.
 - Begin tuning with the SQUID array, similar to a single stage SQUID. Apply a generator signal on Φ_X , with bias signals on I_B and V_B .
 - Optional: Measure the I - Φ and V - Φ characteristic of the SQUID array. How do they compare to the single SQUID?
 - Tune the first stage while the array is at its optimal working point. Apply a generator on Φ_B . Set I to the value with the largest swing of the single SQUID and center U_{OUT} with Φ_X .
- **Analysis:** Plot the V - Φ characteristic of the two stage SQUID in the open loop with Python.
- **Measurement:** Measure and save a noise spectrum with the lowest frequency range that includes a clear cut-off from the SQUID readout.
 - Turn off the generator and activate the flux-locked-loop mode ($R_f = 100 \text{ k}\Omega$). Move U_{OUT} to zero with Φ_B .
 - Switch the oscilloscope to spectrum mode and choose logarithmic axes. You expect two cut-offs: one from the noise thermometer and one from the SQUID readout, affected by the gain-bandwidth-product.
 - Set the gain-bandwidth-product to the highest possible value without resonances.
- **Analysis:** Determine the temperature of the noise thermometer with a fit.
 - You can convert U in dBV to the noise amplitude spectral density $\sqrt{S_V}$ in $\text{V}/\sqrt{\text{Hz}}$ with $\sqrt{S_V} = 10^{U/20}/\sqrt{\Delta f}$ where Δf is the frequency step between the data points.
 - Use the earlier determined amplification to convert $\sqrt{S_V}$ to the noise amplitude spectral density of the current in the input coil $\sqrt{S_I}$ in $\text{A}/\sqrt{\text{Hz}}$
 - Fit the square-root of the noise power spectral density S in $\text{A}^2 \text{Hz}^{-1}$ to the noise amplitude spectral density $\sqrt{S_I}$ to determine the temperature.
 - Assume an input coil inductance of 2.9 nH .

6 Outlook

6.1 State of the art noise thermometers

In this part, the state of the art cross-correlated current noise thermometer is explained. This section is not required for carrying out the lab course, but you may get some nice insights to an ongoing development process. One type of state of the art noise thermometers used in low temperature labs are so called cross-correlated current noise thermometers, short C3NT. This type of noise thermometers are measuring the thermal noise of on resistor that is thermally connected to a experiment. A example for such a thermometer is shown in figure 24.

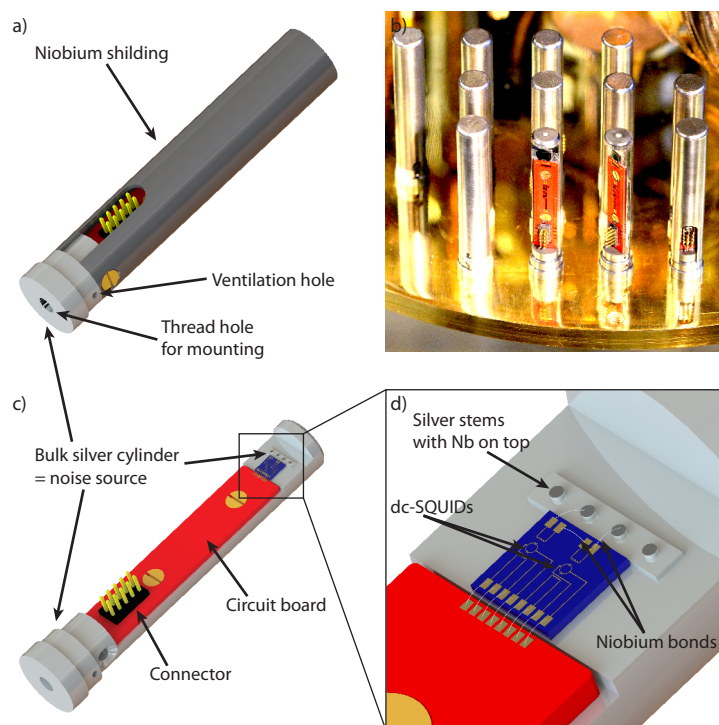


Figure 24: a) Schematic drawing of the C3NT sensor unit with the niobium shielding on top of the silver cylinder. b) Twelve C3NT temperature sensors mounted on the experimental platform of a dilution refrigerator. For the sake of clarity the wires connecting this first stage temperature sensor to the second stage amplifier are not shown. c) The sensor unit without the niobium shielding. d) The input coils of the first stage SQUIDs are connected directly to the noise source by niobium bonding wires.

It should be mentioned that the temperature sensor shown in figure 24 only hosts the first stage SQUIDs, but not the second stage amplifier units. This is due to the fact that,

as already described above, most of the heat is produced within the amplifier unit, what would be unfavorable to be dissipated onto the temperature sensor.

The temperature sensor shown in figure 24, is a massive silver cylinder made from high purity silver. This silver is used as noise source and as mounting for the primary SQUIDs. The reasons why silver is used as noise source is the fact that the heat capacity of silver is rather small at low temperatures, it can be prepared to have a marginal temperature dependency of its receptivity at low temperatures $\Delta\rho(T)/\rho_0 < 10^{-3}$ at $T < 4K$ and it is chemically fairly inert.

With the thermometers shown in figure 24 the noise of the noise source is measured with two identically amplification chains in parallel. This feature allow a more precise temperature measurement, as it is possible to apply the so called cross-correlation to the two signal. This cross-correlation is capable of reducing the amplifier noise to a marginal level.

A schematic drawing, how one such cross-correlated current noise thermometer is read out is displayed in figure 25.

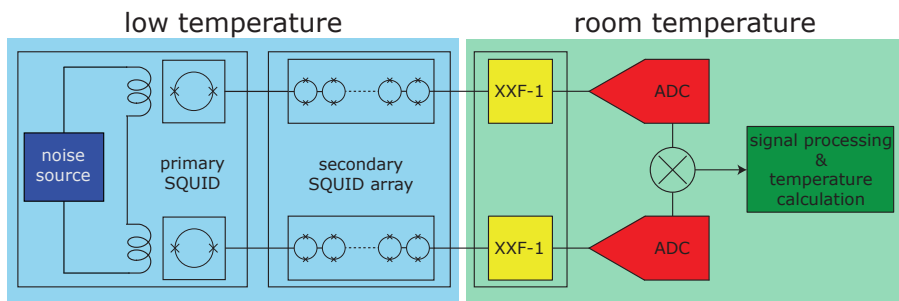


Figure 25: Schematic drawing of the readout scheme used to measure the thermal current noise of a resistor. The noise source is connected to two coils. These two coils are serving as the input coils for two SQUIDS. Each of these primary SQUIDS is operated in a two-stage setup, followed by a secondary SQUID array. This array is then read out by an FLL electronics whose output signal is digitized by an A/D-converter.

Figure 25 gives an overview of the readout scheme of a state of the art C3NT. The noise source (an ohmic resistor) is connected to the input coils of two dc-SQUID two stage setups. From the point on, were the noise signal is coupled to the two primary SQUIDS the analog part of the amplification chain, so until the signal is digitized by the ADC, are independent from each other. The two two stage SQUID setups are operated using a XXF-1 FLL electronics, whose output signal is than digitized and afterwards used for the temperature calculation which is described in the following.

6.1.1 Signal processing of the C3NT

After the digitization, the signal is Fourier-transformed using the Fast-Fourier-Transform (FFT) algorithm. To calculate the FFT and to avoid artefacts, it is necessary to

multiply the original voltage signal by a window function.

Before and after the FFT two methods of cross-talk reduction are discussed. At first the cross-correlation of the two noise spectra measured with the two independent amplifier chains is explained. After that, a mathematical way to reduce the cross-talk via the input circuit is described. At the end of this section, the method used to calculate the temperature and the uncertainty it is loaded with, is explained.

Reduction of parasitic noise by using cross-correlation

In section 2.2.2, the expected power spectral density of a resistor connected to the input coil of a frontend SQUID is explained and derived. In addition to this theory it should be noted that the PSD of a single channel measurement is strongly influenced by the apparent flux noise of the SQUIDs. Since, in case of the C3NT shown in figure ??, the current noise of the resistor is measured simultaneously with two amplifier chains that are nominally independent of each other, it is possible to apply the method of cross correlation.

Applying the cross-correlation onto two simultaneously measured power spectral densities of the same noise source allows to suppress the noise of the room temperature electronics. In this way, the pure noise of the noise resistor could theoretically be filtered out of the measured signals. The cross-correlation is applied to the two Fourier-transformed noise spectra of both channels. To be able to apply the cross-correlation, the following assumptions must be made:

- The noise contribution of the noise source to both noise spectra is identical.
- The noise contribution to the noise spectra of both room temperature amplifiers is completely independent of each other.

With both assumptions being fulfilled, the frequency-dependent complex-valued power spectral densities of both single channels are given by

$$\tilde{u}_1(f) = \tilde{a}(f) + \tilde{n}_1(f) \quad (53)$$

$$\tilde{u}_2(f) = \tilde{a}(f) + \tilde{n}_2(f). \quad (54)$$

Here, the component $\tilde{a}(f)$ denotes the contribution of the noise resistor to the overall noise, while the two components $\tilde{u}_1(f)$ and $\tilde{u}_2(f)$ are representing the parasitic noise contributions of the two amplifier chains.

The cross-correlated power spectral density of the two spectra (53) and (54) is calculated by multiplying one of those spectra with the complex conjugated of the other one:

$$\tilde{u}_1(f) \tilde{u}_2^*(f) = \tilde{a}(f) \tilde{a}^*(f) + \tilde{a}(f) \tilde{n}_2^*(f) + \tilde{a}(f) \tilde{n}_1^*(f) + \tilde{n}_1^*(f) \tilde{n}_2^*(f). \quad (55)$$

If the assumptions from above are fulfilled, the real part of equation 55 simplifies in the limit of very long measurement times to

$$\text{Re}(\tilde{u}_1(f)\tilde{u}_2^*(f)) \xrightarrow{\Delta t \rightarrow \infty} \tilde{a}(f)\tilde{a}^*(f) = S_a(f) \quad (56)$$

The left part in this equation represents the real part of the cross-correlation of the two signals while the right side is the undisturbed power spectral density of the noise to be measured.

Theoretically, it is possible to suppress all noise contributions that do not originate from the noise source itself. However, this is not the case, in case of crosstalk between the two readout chains this leads to additional correlated noise that can not be removed by cross-correlation. The next section will explain a mathematical way to reduce the effect of the crosstalk between the two amplifier chains.

Mathematical suppression of crosstalk

It was already mentioned that there is a certain percentage of noise that is coupled from the one SQUID to the other one via the input circuit and that this crosstalk could be reduced by changing the input circuit of the thermometer. An additional method to calculate the crosstalk and subtract it from the power spectral densities is described in the following.

Assuming an additional crosstalk component that is present in the Fourier-transformed signals of both channels and the remaining crosstalk being equal in either direction, the transformed signals could be approximated in first order by

$$\tilde{s}_1(f) = (1 - \epsilon)\tilde{u}_1(f) + \epsilon\tilde{u}_2(f) \quad (57)$$

$$\tilde{s}_2(f) = (1 - \epsilon)\tilde{u}_2(f) + \epsilon\tilde{u}_1(f). \quad (58)$$

The components $\tilde{u}_1(f)$ and $\tilde{u}_2(f)$ are the ideal crosstalk-free single readout channels power spectral densities whose composition is already described in equation 53 and 54. This system of equations could be solved to find a formula for $\tilde{u}_1(f)$ and $\tilde{u}_2(f)$, resulting in

$$\tilde{u}_1(f) = \frac{-\tilde{s}_1(f) + \epsilon(\tilde{s}_1(f) + \tilde{s}_2(f))}{2\epsilon - 1} \quad (59)$$

$$\tilde{u}_2(f) = \frac{-\tilde{s}_2(f) + \epsilon(\tilde{s}_1(f) + \tilde{s}_2(f))}{2\epsilon - 1} \quad (60)$$

where the crosstalk is subtracted.

To obtain this result it was necessary to assume that $\epsilon - 1 \neq 0$ and $2\epsilon - 1 \neq 0$ holds for all possible values of ϵ . As ϵ is the crosstalk between the two SQUID channels which has a value of less than 0.1, even for the case of the input coils connected in series, it is no problem to fulfil these requirements.

Determining the noise temperature

After Fourier-transforming both signals, correcting them for crosstalk and doing the cross correlation to calculate the power spectral density, the obtained noise spectra are used to calculate the temperature.

The noise thermometers discussed in this thesis are operated as relative primary thermometers. This technical term wants to express that the thermometers require only one point of calibration to be able to measure the temperature over a wide range. To do this calibration a calibration spectrum $S_{\text{cal}}(f)$ is recorded at a known calibration temperature T_{cal} .

Using a recorded power spectral density $S(f)$, the calibration spectrum and the calibration temperature, the temperature corresponding to the recorded power spectral density is given by

$$T = \frac{S(f)}{S_{\text{cal}}(f)} T_{\text{cal}}. \quad (61)$$

In the algorithm used to calculate the temperature T , single frequency bins are used to calculate a spectrum of temperatures, hence equation 61 changes to

$$T_i = \frac{S_i(f_i)}{S_{i,\text{cal}}(f_i)} T_{\text{cal}}. \quad (62)$$

In the next step, the sequence T_i of temperatures is averaged over the range of reliable frequencies to retrieve one temperature value.

The fact that both measured power spectral densities are loaded with a statistical uncertainty results in a systematic and a statistical uncertainty of the calculated temperature value. Both types of deviations will be discussed in the following, starting with the systematic one.

Systematic uncertainty

The contribution to the systematic uncertainty discussed here is a result of the statistical uncertainty of the calibration power spectral density $S_{\text{cal}}(f)$. This kind of systematic uncertainty is occurring if a calculated value is inverse proportional to the measured value that is loaded with a statistical uncertainty, as it is the case for the temperature calculated by formula 60. This fact leads to the systematic uncertainty

$$\Delta_{\text{sys}} = \frac{\Delta T_{\text{syst}}}{T} = \left[1 - \frac{1}{1 - \Delta_{\text{stat,cal}}} \right] - \left[1 - \frac{1}{1 + \Delta_{\text{stat,cal}}} \right], \quad (63)$$

containing $\Delta_{\text{stat,cal}} = \Delta S_{\text{cal}}/S_{\text{cal}}$, the relative statistical uncertainty of the calibration spectrum. Of course, the value of $\Delta_{\text{stat,cal}}$, varies to smaller values as often as it varies to higher values, which leads to a different deviation of the calculated temperature. Varying to a higher value results in a smaller deviation of the calculated temperature, than an identical fluctuation of the calibration spectrum to a lower value.

The systematic uncertainty described by formula 63 can be simplified to

$$\Delta_{\text{sys}} = \frac{\Delta T_{\text{sys}}}{T} = \frac{2}{\frac{1}{\Delta S_{\text{stat,cal}}^2} - 1} = \frac{2}{\left(\frac{S_{\text{stat,cal}}}{\Delta S_{\text{stat,cal}}}\right)^2 - 1}. \quad (64)$$

As this formula states, it is crucial to have the lowest possible statistical uncertainty of the calibration spectrum, which of course decreases with an increasing number of averages made for acquiring this spectrum. This also leads to the conclusion that the calibration spectrum should be recorded with a rather long measurement time.

Statistic uncertainty

So far only the statistical uncertainty of the calibration spectrum was considered, but of course the power spectral density $S(f)$ of each single temperature measurement is also loaded with a statistical uncertainty. This statistical uncertainty is higher than the statistical uncertainty of the calibration spectrum as the measurement time is much shorter. As mentioned during the discussion of the systematic uncertainty on the calculated temperature value, the statistical uncertainty of the calibration spectrum is desired to be as small as possible, hence it is assumed to be negligible compared to the statistical uncertainty of the spectrum $S(f)$.

For $S(f)$ it is true that the statistical uncertainty of the calculated temperature $T(f_i)$ of a certain frequency bin is inverse proportional to the square root of the averaged number N of single spectra used for the measurement of this spectrum:

$$\Delta_{\text{stat,i}} = \frac{\Delta T_{\text{stat,i}}}{T_i} = \left(\frac{1}{N}\right)^{\frac{1}{2}}. \quad (65)$$

It was already mentioned that the used frequency bandwidth $[f_0, f_0 + \Delta f]$ is split up in M smaller frequency bands with δf , hence a number of $M = \Delta f / \delta f$ frequency bands are used to calculate the temperature, resulting in a sequence of M temperatures that are averaged.

Taking all these facts together, the statistical uncertainty of the calculated temperature value is given by

$$\begin{aligned} \frac{\Delta T}{T} &= \frac{\Delta T_i}{T_i} \left(\frac{1}{M}\right)^{\frac{1}{2}} = \left(\frac{1}{N}\right)^{\frac{1}{2}} \left(\frac{1}{\frac{\Delta f}{\delta f}}\right)^{\frac{1}{2}} \\ &= \left(\frac{1}{t\Delta f}\right)^{\frac{1}{2}}. \end{aligned} \quad (66)$$

Within this equation, the total length of the measurement is represented by $t = N\tau$, whereas $\tau = 1/\delta f$ defines the length of one single spectrum.

Using the assumption made for the statistical uncertainty of the calibration spectra to calculate the statistical uncertainty given by equation 65, it is possible to evaluate the

relevancy of the systematic uncertainty described above. For equation 65 it was assumed to have a calibration measurement that was recorded over quite a long time. Due to the fact that the systematic deviation can easily be reduced to such a small value, it can be neglected.

References

- [1] C. J. Borkowski and T. V. Blalock. A new method of Johnson noise thermometry. *Rev. Sci. Instrum.*, 45(2):151–162, 1974.
- [2] R. Brown. XXVII. A brief account of microscopical observations made in the months of June, July and August 1827, on the particles contained in the pollen of plants; and on the general existence of active molecules in organic and inorganic bodies. *Philos. Mag.*, 4(21):161–173, sep 1827.
- [3] J. Clarke and A. I. Braginski. *The SQUID handbook. Vol. 1, Fundamentals and technology of SQUIDs and SQUID systems*. Weinheim : Wiley-VCH, 2004.
- [4] A. Einstein. Über die von der molekularkinetischen Theorie der Wärme geforderte Bewegung von in ruhenden Flüssigkeiten suspendierten Teilchen. *Ann. Phys.*, 322(8):549–560, 1905.
- [5] C. Enss and S. Hunklinger. *Low Temperature Physics*. Springer Verlag, Heidelberg, 2005.
- [6] A. Ferring. Entwicklung von dc-squids zur auslesung von metallischen magnetischen kalorimetern. Master thesis, Kirchhoff Institute for Physics, Heidelberg University, March 2015.
- [7] A. Fleischmann, A. Reiser, and C. Enss. Noise Thermometry for Ultralow Temperatures. *J. Low Temp. Phys.*, 201(5-6):803–824, 2020.
- [8] Rudolf Gross, Achim Marx, Dietrich Einzel, and Stephan Geprägs. *Festkörperphysik*. De Gruyter Studium. De Gruyter, Berlin ; Boston, 2. auflage edition, 2018. 1. Auflage verfasst von Rudolf Gross, Achim Marx und Dietrich Einzel ; "Neu in der 2. Auflage: Vier vollkommen neue und zahlreiche überarbeitete Aufgaben" - hinterer Umschlag.
- [9] J. B. Johnson. Thermal Agitation of Electricity in Conductors. *Nature*, 119(2984):50–51, 1927.
- [10] J. B. Johnson. Thermal agitation of electricity in conductors. *Phys. Rev.*, 32(1):97–109, 1928.
- [11] H. Nyquist. Thermal agitation of electric charge in conductors. *Phys. Rev.*, 32:110–113, Jul 1928.
- [12] C. Staender. Compact, fast and reliable cross-correlated current noise thermometers for milli- and micro-kelvin temperatures. Master thesis, Kirchhoff Institute for Physics, Heidelberg University, December 2020.
- [13] D. Unger. Development and characterization of a high energy resolution and low background detector module for the IAXO experiment. Master thesis, Kirchhoff Institute for Physics, Heidelberg University, March 2020.